Adaptive Anti-vibration Boundary Control for a Hovering Three-dimensional Helicopter Flexible Slung-load System with Input Saturation and Backlash

Yong Ren, *Member, IEEE*, Zhijie Liu, *Member, IEEE*, Zhijia Zhao, *Member, IEEE*, and Hak-Keung Lam, *Fellow, IEEE*

***Abstract*—This study investigates anti-swing control for a hovering three-dimensional helicopter flexible slung-load system (HFSLS) subject to input saturation and backlash. The first target of the study is to establish a new model for a hovering three-dimensional HFSLS. The second target is to develop an adaptive control law for a HFSLS by analyzing its ability to compensate for the effects of input saturation, input backlash, and external disturbances, while achieve the goal of vibration reduction. In contrast to existing research, adaptive boundary control technology was first introduced to solve the oscillation suppression problem and validated using numerical simulation of the HFSLS and the proposed control method. The proposed control method is discussed, and the PD control method was compared.**

***Index Terms*—Adaptive boundary control, anti-vibration, three-dimensional helicopter flexible slung-load system, input saturation, input backlash.**

I. Introduction

THE helicopter slung-load system plays an increasingly important role in modern society. Current research is aimed at the rigid-body model of a helicopter slung-load system [1]-[4] with little focus on helicopter flexible slung-load systems (HFSLS) [5]-[7]. However, these studies were meant for a horizontal model of the HFSLS. Thus, vibration suppression control for three-dimensional HFSLS is required.

Numerous effective vibration reduction control methods have been proposed [8]-[19]. In [20], a new adaptive boundary control scheme was introduced to investigate the anti-swing control design problem of a flexible Timoshenko system. The effects of compensating for actuator failures, backlash-like hysteresis, and external disturbances were remedied simultaneously. For a flexible wind turbine tower, the problems of vibration and disturbance rejection were studied using boundary technology in [21]. Under the developed control design, the scope of the vibration can remain in a small compact set; however, to solve the asymmetric input-output constraint, the authors introduced auxiliary systems and barrier Lyapunov functions for flexible rotary crane systems in [22]. The authors in [23] adopted boundary feedback control to suppress the vibration of a flexible air-breathing hypersonic vehicle system described by a set of distributed parameter systems. Based on the above analysis, the boundary control strategy was efficient for stability analysis of flexible structure systems. Thus, we adopt a boundary control method to investigate the control problem for a three-dimensional HFSLS.

Constraint problems are common phenomena in engineering, and several outstanding research goals have been achieved [24]-[33]. Based on the auxiliary design and disturbance observer method, the problems of input saturation and external disturbances were addressed for hypersonic flight vehicles in [34]. In [35], output feedback control was studied for a flexible manipulator modelled by a partial differential equation model, in which an adaptive backlash inverse function was utilized to handle the unknown input backlash. In [36], the trajectory tracking control problem was researched for robot manipulators, and a neural network technique was employed to handle input saturation. The authors proved the uniform ultimate boundedness of nonlinear systems using a fuzzy robust constrained control in [37], in which a sigmoid function and fuzzy logic systems were used to address input saturation. However, to the best of the author's knowledge, the mixed impacts of input saturation and input backlash were not considered for flexible structure systems.

In this study, a three-dimensional HFSLS subjected to input saturation and input backlash was established using a set of partial differential equations. To reduce the number of calculations resulting from addressing input saturation and input backlash separately, the two functions were transformed into a new saturation function. Subsequently, the method of auxiliary system design was adopted to compensate for the effect of the new saturation function. A novel adaptive boundary control scheme using the designed auxiliary systems was introduced to ensure that the closed-loop system of the three-dimensional HFSLS is semi-uniformly ultimately bounded.

These innovations are reflected in the following three aspects:

- A new model for a three-dimensional HFSLS is proposed,

Y. Ren is with the College of Electrical Engineering and Automation, Shandong University of Science and Technology, Qingdao 266590, China (e-mail: renyong@sdust.edu.cn).

Z. Liu is with the School of Automation and Electrical Engineering, and Institute of Artificial Intelligence, University of Science and Technology Beijing, Beijing 100083, China (e-mail: liuzhijie2012@gmail.com).

Z. Zhao is with the School of Mechanical and Electrical Engineering, Guangzhou University, Guangzhou 510006, China (e-mail: zhjzhaoscut@163.com).

H.-K. Lam is with the Department of Engineering, King's College London, London, WC2R 2LS, U.K. (email: hak-keung.lam@kcl.ac.uk).

which is defined by a set of partial differential equations;

- The two functions of input saturation and backlash are transformed into a new saturation function in order to reduce computation complexity;
- Finally, a novel adaptive boundary control law is designed to compensate for the effects of input saturation, input backlash, and external disturbances for the HFSLS. Meanwhile, the objective of reducing vibration is came true.

Notations: $\min\{s_1, s_2, \cdots, s_n\}$ is used to calculate the minimum value among s_1, s_2, $\cdots$, s_n. $\max\{s_1, s_2, \cdots, s_n\}$ is employed to acquire the maximum value among s_1, s_2, $\cdots$, s_n. For simplicity, we give the following definitions: $\dot{(\cdot)} = \frac{\partial(\cdot)}{\partial t}$, $\ddot{(\cdot)} = \frac{\partial^2(\cdot)}{\partial t^2}$, $(\cdot)' = \frac{\partial(\cdot)}{\partial r}$, $(\cdot)'' = \frac{\partial^2(\cdot)}{\partial r^2}$, and $\dot{(\cdot)}' = \frac{\partial^2(\cdot)}{\partial r \partial t}$, $\forall r \in [0, l]$, $t \in [0, \infty)$.

II. Problem Formulation and Preliminaries

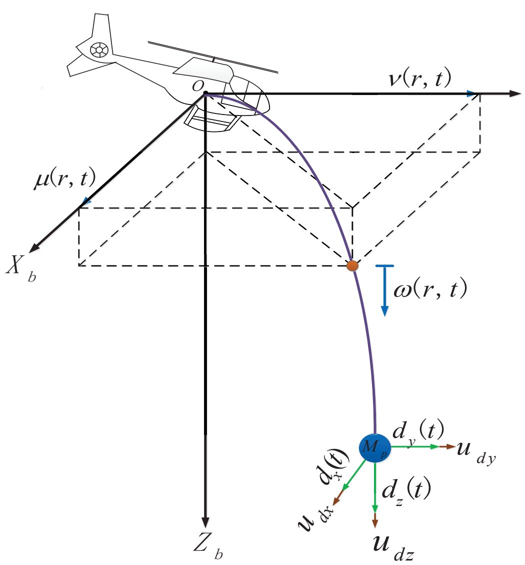

Fig. 1: A diagram for a hovering three-dimensional HFSLS.

A three-dimensional diagram of a hovering HFSLS is shown in Fig. 1. Here, $\mu(r,t)$ and $\nu(r,t)$ denote the lateral displacements in the X_b and Y_b coordinates, respectively, and $\omega(r,t)$ represents the longitudinal displacement in the Z_b coordinate. A mathematical model for the HFSLS is established using the extended Hamiltonian principle and the detailed modelling process is as follows.

The kinetic energy $W_e(t)$ of the HFSLS is described by:

$$
\begin{aligned}
W_e(t) &= \frac{\varpi}{2}\int_0^l \Big[\mu^2(r,t) + \nu^2(r,t) + \omega^2(r,t)\Big]dr \\
&\quad + \frac{M_p}{2}\Big[\mu^2(l,t) + \nu^2(l,t) + \omega^2(l,t)\Big], \qquad (1)
\end{aligned}
$$

where M_p and ϖ denote the mass of the load and mass per unit length of the slung string, respectively. By applying the variation operator δ to Equation (1), we obtain:

$$
\begin{aligned}
&\int_{t_1}^{t_2} \delta W_e(t)dt \\
= \;& \varpi \int_{t_1}^{t_2}\int_0^l \Big[\mu(r,t)\delta\mu(r,t) + \nu(r,t)\delta\nu(r,t) + \omega(r,t) \\
& \times\delta\omega(r,t)\Big]dxdt + M_p\int_{t_1}^{t_2}\Big[\mu(l,t)\delta\mu(l,t) + \nu(l,t) \\
& \times\delta\nu(l,t) + \omega(l,t)\delta\omega(l,t)\Big]dt \\
= \;& \varpi \int_{t_1}^{t_2}\int_0^l \Big[\ddot{\mu}(r,t)\delta\mu(r,t) + \ddot{\nu}(r,t)\delta\nu(r,t) + \ddot{\omega}(r,t) \\
& \times\delta\omega(r,t)\Big]dxdt - M_p\int_{t_1}^{t_2}\Big[\ddot{\mu}(l,t)\delta\mu(l,t) + \ddot{\nu}(l,t) \\
& \times\delta\nu(l,t) + \ddot{\omega}(l,t)\delta\omega(l,t)\Big]dt. \qquad (2)
\end{aligned}
$$

The potential energy $W_p(t)$ of the HFSLS is expressed as

$$
\begin{aligned}
W_p(t) &= \frac{EA}{2}\int_0^l \Big[\frac{[\mu'(r,t)]^2}{2} + \frac{[\nu'(r,t)]^2}{2} + \omega'(r,t)\Big]^2 dr \\
&\quad + \frac{T}{2}\int_0^l [\mu'(r,t)]^2 + [\nu'(r,t)]^2 dr, \qquad (3)
\end{aligned}
$$

where EA and T are the axial stiffness and tension of the slung string, respectively. Similarly, by applying the variation operator δ to Equation (3), we derive:

$$
\begin{aligned}
&\int_{t_1}^{t_2} \delta W_p(t)dt \\
= \;& \int_{t_1}^{t_2} \delta\Big\{\frac{EA}{2}\int_0^l \Big[\frac{[\mu'(r,t)]^2}{2} + \frac{[\nu'(r,t)]^2}{2} \\
& +\omega'(r,t)\Big]^2 dr + \frac{T}{2}\int_0^l [\mu'(r,t)]^2 + [\nu'(r,t)]^2 dr\Big\}dt \\
= \;& EA\int_{t_1}^{t_2}\int_0^l \Big[\frac{[\mu'(r,t)]^2}{2} + \frac{[\nu'(r,t)]^2}{2} + \omega'(r,t)\Big]dr \\
& \times\delta\Big\{\int_0^l \Big[\frac{[\mu'(r,t)]^2}{2} + \frac{[\nu'(r,t)]^2}{2} + \omega'(r,t)\Big]dr\Big\}dt \\
& +T\int_0^l \mu'(r,t)\delta[\mu'(r,t)] + \nu'(r,t)\delta[\nu'(r,t)]dr\Big\}dt \\
= \;& -\int_{t_1}^{t_2}\int_0^l \Big\{T\mu''(r,t) + \frac{3EA}{2}[\mu'(r,t)]^2\mu''(r,t) \\
& +EA[\mu'(r,t)\omega''(r,t) + \mu''(r,t)\omega'(r,t)] + \frac{EA}{2} \\
& \times\Big[\mu''(r,t)[\nu'(r,t)]^2 + 2\mu'(r,t)\nu'(r,t)\nu''(r,t)\Big]\Big\} \\
& \times\delta\mu(r,t) + \Big\{T\nu''(r,t) + \frac{3EA}{2}[\nu'(r,t)]^2\nu''(r,t) \\
& +EA[\nu'(r,t)\omega''(r,t) + \nu''(r,t)\omega'(r,t)] + \frac{EA}{2} \\
& \times\Big[\nu''(r,t)[\mu'(r,t)]^2 + 2\nu'(r,t)\mu'(r,t)\mu''(r,t)\Big]\Big\} \\
& \times\delta\nu(r,t) + \Big\{EA\omega''(r,t) + EA\mu'(r,t)\mu''(r,t) \\
& +EA\nu'(r,t)\nu''(r,t)\Big\}\delta\omega(r,t)drdt + \int_{t_1}^{t_2}\Big\{T\mu'(l,t)
\end{aligned}
$$

$$
+\frac{EA}{2}[\mu'(l,t)]^3+EA\mu'(l,t)\omega'(l,t)+\frac{EA}{2}\mu'(l,t)
\times[\nu'(l,t)]^2\Big\}\delta\mu(l,t)+\Big\{T\nu'(l,t)+\frac{EA}{2}[\nu'(l,t)]^3
+EA\nu'(l,t)\omega'(l,t)+\frac{EA}{2}\nu'(l,t)[\mu'(l,t)]^2\Big\}\delta\nu(l,t)
+\Big\{EA\omega'(l,t)+\frac{EA}{2}[\mu'(l,t)]^2+\frac{EA}{2}[\nu'(l,t)]^2\Big\}
\times\delta\omega(l,t). \tag{4}
$$

Virtual work done by the distributed loads $u_x(r,t)$, $u_y(r,t)$, and $u_z(r,t)$ on the slung string and the external disturbances $d_x(t)$, $d_y(t)$, and $d_z(t)$ on the load is expressed as follows:

$$
\begin{aligned}
\delta W_1(t) &= \int_0^l \Big[u_{dx}(r,t)\delta\mu(r,t)+u_{dy}(r,t)\delta\nu(r,t) \\
&\quad +u_{dz}(r,t)\delta\omega(r,t)\Big]dr+d_x(t)\delta\mu(l,t) \\
&\quad +d_y(t)\delta\nu(l,t)+d_z(t)\delta\omega(l,t),
\end{aligned} \tag{5}
$$

where δ denotes a variational operator. The work performed by the control inputs is as follows:

$$
\begin{aligned}
\delta W_2(t) &= u_x(t)\delta\mu(l,t)+u_y(t)\delta\nu(l,t) \\
&\quad +u_z(t)\delta\omega(l,t).
\end{aligned} \tag{6}
$$

Combining (5) and (6), the total virtual work performed on the HFSLS is described as follows:

$$
\begin{aligned}
\delta W(t) &= \delta W_1(t)+\delta W_2(t) \\
&= \int_0^l \Big[u_{dx}(r,t)\delta\mu(r,t)+u_{dy}(r,t)\delta\nu(r,t) \\
&\quad +u_{dz}(r,t)\delta\omega(r,t)\Big]dr+[u_x(t)+d_x(t)] \\
&\quad \times\delta\mu(l,t)+[u_y(t)+d_y(t)]\delta\nu(l,t) \\
&\quad +[u_z(t)+d_z(t)]\delta\omega(l,t).
\end{aligned} \tag{7}
$$

From the extended Hamiltonian principle, $\int_{t_1}^{t_2}\delta[W_e(t)-W_p(t)+W(t)]dt=0$ where $0<t_1<t<t_2$, t_1 and t_2 are two time constants [38], defining $\mu=\mu(r,t)$, $\nu=\nu(r,t)$, $\omega=\omega(r,t)$, $\mu_l=\mu(l,t)$, $\nu_l=\nu(l,t)$, $\omega_l=\omega(l,t)$, and $u_{dk}=u_{dk}(r,t)$, $k=x,y,z$, we derive the three-dimensional HFSLS in hovering as follows:

$$
\begin{aligned}
\varpi\ddot{\mu} &= T\mu''+\frac{3EA}{2}[\mu']^2\mu''+EA[\mu'\omega''+\mu''\omega'] \\
&\quad +\frac{EA}{2}\Big\{\mu''[\nu']^2+2\mu'\nu'\nu''\Big\}+u_{dx}, && (8)\\
\varpi\ddot{\nu} &= T\nu''+\frac{3EA}{2}[\nu']^2\nu''+EA[\nu'\omega''+\nu''\omega'] \\
&\quad +\frac{EA}{2}\Big\{\nu''[\mu']^2+2\mu'\mu''\nu'\Big\}+u_{dy}, && (9)\\
\varpi\ddot{\omega} &= EA\omega''+EA\mu'\mu''+EA\nu'\nu''+u_{dz}, && (10)
\end{aligned}
$$

under the following boundary conditions:

$$
\begin{aligned}
&\mu(0,t)=\nu(0,t)=\omega(0,t)=0, && (11)\\
&M_p\ddot{\mu}_l=-T\mu_l'-\frac{EA}{2}[\mu_l']^3-EA\mu_l'\omega_l'-\frac{EA}{2}\mu_l'[\nu_l']^2 \\
&\qquad +u_x(t)+d_x(t), && (12)\\
&M_p\ddot{\nu}_l=-T\nu_l'-\frac{EA}{2}[\nu_l']^3-EA\nu_l'\omega_l'-\frac{EA}{2}\nu_l'[\mu_l']^2 \\
&\qquad +u_y(t)+d_y(t), && (13)\\
&M_p\ddot{\omega}_l=-EA\omega_l'-\frac{EA}{2}[\mu_l']^2-\frac{EA}{2}[\nu_l']^2+u_z(t) \\
&\qquad +d_z(t). && (14)
\end{aligned}
$$

Input saturation and backlash, which are common in mechanical actuators, are considered in this study and the saturation function is given by [24]:

$$
u_{kb}(t)=\mathrm{S}(\vartheta_k(t))=\begin{cases}\vartheta_{kM}, & \text{if } \vartheta_k(t)\ge\vartheta_{kM},\\ \vartheta_k(t), & \text{if } \vartheta_{km}<\vartheta_k(t)<\vartheta_{kM},\\ \vartheta_{km}, & \text{if } \vartheta_k(t)\le\vartheta_{km},\end{cases} \tag{15}
$$

where $\mathrm{S}(\cdot)$ is the saturation function and $\vartheta_{kM}>0$ and $\vartheta_{km}<0$ denote the saturation levels of the control input $\varrho_k(t)$ and $k=x,y,z$. The backlash function is described by [35]:

$$
u_k(t)=\mathcal{B}(u_{kb}(t))=\begin{cases}\xi_k(u_{kb}(t)-\iota_{kr}), & \text{if } \dot{u}_{kb}(t)>0\\ & \quad\text{and } u_k(t)=\xi_k(u_{kb}(t)-\iota_{kr}),\\ \xi_k(u_{kb}(t)+\iota_{kl}), & \text{if } \dot{u}_{kb}(t)<0\\ & \quad\text{and } u_k(t)=\xi_k(u_{kb}(t)+\iota_{kl}),\\ u_k(t_-), & \text{otherwise},\end{cases} \tag{16}
$$

where $\mathcal{B}(\cdot)$ is the input backlash function, $u_{kb}(t)$ denotes the desired control input, $\xi_k>0$ represents the slope of $\mathcal{B}(\cdot)$, $\iota_{kr}>0$ and $\iota_{kl}>0$ indicate backlash spacing, and $u_k(t_-)=u_k(t)$ and $k=x,y,z$.

According to [39], we define the following right inverse function $\mathcal{B}^+(\cdot)$ of $\mathcal{B}(\cdot)$:

$$
\vartheta_k(t)=\mathcal{B}^+(\chi_k(t))=\begin{cases}\chi_k(t)/\xi_k+\iota_{kr}, & \text{if } \dot{u}_{kb}(t)>0,\\ \chi_k(t)/\xi_k-\iota_{kl}, & \text{if } \dot{u}_{kb}(t)<0,\\ \chi_k(t_-), & \text{otherwise},\end{cases} \tag{17}
$$

where $k=x,y,z$.

Based on the above definitions, we can conclude that

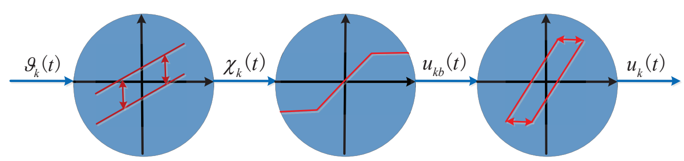

Fig. 2: Saturation and backlash nonlinearities integrated with $\mathcal{B}^+(\cdot)$.

From Fig. 2, mixed input nonlinearity, which is constituted by input saturation and input backlash is depicted by:

$$
u_k(t)=\mathcal{B}(\mathrm{S}(\mathcal{B}^+(\vartheta_k(t))))=\begin{cases}\xi_k(\vartheta_{kM}-\iota_{kr})\\ \text{if } \vartheta_k(t)\ge\xi_k(\vartheta_{kM}-\iota_{kr}),\\ \xi_k(\vartheta_{km}+\iota_{kl})\\ \text{if } \vartheta_k(t)\le\xi_k(\vartheta_{km}+\iota_{kl}),\\ u_k(t_-), \ \text{otherwise}.\end{cases} \tag{18}
$$

Hence, the input nonlinearity function, which includes a saturation function and input backlash function, can be transformed into a new saturation function.

The following assumptions and lemma are required for the stability proof.

Assumption 1 [8]: The distributed loads u_{dx}, u_{dy}, and u_{dz} satisfy $|u_{dk}| \leq \bar{u}_k$ where $\bar{u}_k > 0$ denotes a constant and $k = x, y, z$. Meanwhile, the disturbance $d_k(t)$ acting on the load is bounded, that is, $|d_k(t)| \leq \bar{D}_k$ where $\bar{D}_k > 0$ denotes a constant and $k = x, y, z$.

Assumption 2 [5]: The new saturation function in (18) satisfies $|\Delta u_k(t)| \leq \varepsilon_k$ where $\Delta u_k(t) = \vartheta_k(t) - u_k(t)$, $\varepsilon_k > 0$ is a constant, and $k = x, y, z$.

Lemma 1 [40]: For a function $\alpha \in \mathcal{C}^1$ on r with $\alpha(0,t) = 0$, we have that

$$\begin{aligned} \alpha^2 &\leq l\int_0^l [\alpha']^2 dr, \\ \alpha\beta &\leq \epsilon\alpha^2 + \frac{1}{\epsilon}\beta^2, \quad \forall r \in [0, l], \end{aligned}$$

where $\alpha = \alpha(r,t)$, $\beta = \beta(r,t)$, $\epsilon > 0$ represents a constant.

Remark 1: Addressing input saturation and backlash directly will be a complex task for a three-dimensional HFSLS. Thus, we transform the input saturation and backlash functions into a new saturation function by defining the right-inverse function: $\mathcal{B}^{+}(\cdot)$ of $\mathcal{B}(\cdot)$.

III. Adaptive Boundary Controller Design and Stability Analysis

First, we adopt the strategy of designing auxiliary systems to address the newly constructed saturation function in (18). Subsequently, an adaptive boundary control scheme was developed for three-dimensional HFSLS based on the proposed auxiliary systems. Under the developed control strategy, a stability analysis is performed for the three-dimensional HFSLS using the direct Lyapunov method.

A. Controller Design

To compensate for the deviation between the control input and actuator output, the auxiliary systems are designed as follows:

$$\begin{aligned} \dot{\delta}_x(t) &= \frac{1}{M_p}\Big\{ -\gamma_x\delta_x(t) + \Delta u_x(t) + T\mu_l' + T\dot{\mu}_l \\ &\quad + \frac{EA}{2}[\mu_l']^3 + EA\mu_l'\omega_l' + \frac{EA}{2}\mu_l'[\nu_l']^2\Big\}, \quad (19) \\ \dot{\delta}_y(t) &= \frac{1}{M_p}\Big\{ -\gamma_y\delta_y(t) + \Delta u_y(t) + T\nu_l' + T\dot{\nu}_l \\ &\quad + \frac{EA}{2}[\nu_l']^3 + EA\nu_l'\omega_l' + \frac{EA}{2}\nu_l'[\mu_l']^2\Big\}, \quad (20) \\ \dot{\delta}_z(t) &= \frac{1}{M_p}\Big\{ -\gamma_z\delta_z(t) + \Delta u_z(t) + EA\omega_l' \\ &\quad + \frac{EA}{2}[\mu_l']^2 + \frac{EA}{2}[\nu_l']^2\Big\}. \quad (21) \end{aligned}$$

Based on the aforementioned auxiliary systems, we define the following new variables:

$$\begin{aligned} \zeta_x(t) &= \dot{\mu}_l + \mu_l' + \delta_x(t), \quad (22) \\ \zeta_y(t) &= \dot{\nu}_l + \nu_l' + \delta_y(t), \quad (23) \\ \zeta_z(t) &= \dot{\omega}_l + \omega_l' + \delta_z(t). \quad (24) \end{aligned}$$

Invoking (12)-(14), (19)-(24), and $\Delta u_k(t) = \vartheta_k(t) - u_k(t)$, where $k = x, y, z$, we have

$$\begin{aligned} \dot{\zeta}_x(t) &= \ddot{\mu}_l + \dot{\mu}_l' + \dot{\delta}_x(t) \\ &= \frac{1}{M_p}\Big\{ -T\mu_l' - \frac{EA}{2}[\mu_l']^3 - EA\mu_l'\omega_l' - \frac{EA}{2}\mu_l'[\nu_l']^2 \\ &\quad + u_x(t) + d_x(t) + M_p\dot{\mu}_l' - \gamma_x\delta_x(t) \\ &\quad + \Delta u_x(t) + T\mu_l' + T\dot{\mu}_l + \frac{EA}{2}[\mu_l']^3 \\ &\quad + EA\mu_l'\omega_l' + \frac{EA}{2}\mu_l'[\nu_l']^2\Big\} \\ &= \frac{1}{M_p}\Big\{\vartheta_x(t) + d_x(t) + M_p\dot{\mu}_l' - \gamma_x\delta_x(t) \\ &\quad + T\dot{\mu}_l\Big\}, \quad (25) \end{aligned}$$

$$\begin{aligned} \dot{\zeta}_y(t) &= \ddot{\nu}_l + \dot{\nu}_l' + \dot{\delta}_y(t) \\ &= \frac{1}{M_p}\Big\{ -T\nu_l' - \frac{EA}{2}[\nu_l']^3 - EA\nu_l'\omega_l' - \frac{EA}{2}\nu_l'[\mu_l']^2 \\ &\quad + u_y(t) + d_y(t) + M_p\dot{\nu}_l' - \gamma_y\delta_y(t) \\ &\quad + \Delta u_y(t) + T\nu_l' + T\dot{\nu}_l + \frac{EA}{2}[\nu_l']^3 \\ &\quad + EA\nu_l'\omega_l' + \frac{EA}{2}\nu_l'[\mu_l']^2\Big\} \\ &= \frac{1}{M_p}\Big\{\vartheta_y(t) + d_y(t) + M_p\dot{\nu}_l' - \gamma_y\delta_y(t) \\ &\quad + T\dot{\nu}_l\Big\}, \quad (26) \end{aligned}$$

and

$$\begin{aligned} \dot{\zeta}_z(t) &= \ddot{\omega}_l + \dot{\omega}_l' + \dot{\delta}_z(t) \\ &= \frac{1}{M_p}\Big\{ -EA\omega_l' - \frac{EA}{2}[\mu_l']^2 - \frac{EA}{2}[\nu_l']^2 + u_z(t) \\ &\quad + d_z(t) + M_p\dot{\omega}_l' - \gamma_z\delta_z(t) + \Delta u_z(t) \\ &\quad + EA\omega_l' + \frac{EA}{2}[\mu_l']^2 + \frac{EA}{2}[\nu_l']^2\Big\} \\ &= \frac{1}{M_p}\Big\{\vartheta_z(t) + d_z(t) + M_p\dot{\omega}_l' - \gamma_z\delta_z(t)\Big\}. \quad (27) \end{aligned}$$

Remark 2: The technology for developing auxiliary systems in (19)-(21), which is a forward compensation method, addresses the input saturation problem.

B. Stability Analysis

To decrease the vibration of a three-dimensional HFSLS with input saturation and backlash, we designed the following adaptive boundary control law:

$$\begin{aligned} \dot{\hat{\bar{D}}}_x(t) &= \psi_x\Big\{\beta_1\zeta_x(t)\tanh\Big(\frac{\zeta_x(t)}{\sigma_x}\Big) - \lambda_x\hat{\bar{D}}_x(t)\Big\}, \quad (28) \\ \dot{\hat{\bar{D}}}_y(t) &= \psi_y\Big\{\beta_1\zeta_y(t)\tanh\Big(\frac{\zeta_y(t)}{\sigma_y}\Big) - \lambda_y\hat{\bar{D}}_y(t)\Big\}, \quad (29) \\ \dot{\hat{\bar{D}}}_z(t) &= \psi_z\Big\{\beta_1\zeta_z(t)\tanh\Big(\frac{\zeta_z(t)}{\sigma_z}\Big) - \lambda_z\hat{\bar{D}}_z(t)\Big\}, \quad (30) \\ \vartheta_x(t) &= -M_p\dot{\mu}_l' - T\dot{\mu}_l - g_x\zeta_x(t) - \frac{EA}{2}[\mu_l']^3 - EA\mu_l'\omega_l' \\ &\quad - \frac{EA}{2}\mu_l'[\nu_l']^2 + \gamma_x\delta_x(t) - \tanh\Big(\frac{\zeta_x(t)}{\sigma_x}\Big)\hat{\bar{D}}_x(t), \end{aligned}$$

$$\vartheta_y(t) = -M_p\dot{\nu}_l' - T\dot{\nu}_l - g_y\zeta_y(t) - \frac{EA}{2}[\nu_l']^3 - EA\nu_l'\omega_l' - \frac{EA}{2}\nu_l'[\mu_l']^2 + \gamma_y\delta_y(t) - \tanh\Big(\frac{\zeta_y(t)}{\sigma_y}\Big)\hat{\bar{D}}_y(t), \tag{31, 32}$$

$$\vartheta_z(t) = -M_p\dot{\omega}_l' - g_z\zeta_z(t) - \frac{EA}{2}[\mu_l']^2 - \frac{EA}{2}[\nu_l']^2 + \gamma_z\delta_z(t) - \tanh\Big(\frac{\zeta_z(t)}{\sigma_z}\Big)\hat{\bar{D}}_z(t), \tag{33}$$

where ψ_k, β_1, σ_k, λ_k, g_k, and l_k are positive constants, and $k = x, y, z$.

In the following section, the semi-uniform boundedness of the HFSLS is proven by employing Lemma 2. First, the following Lyapunov candidate function is chosen:

$$\Upsilon(t) = \Upsilon_1(t) + \Upsilon_2(t) + \Upsilon_3(t), \tag{34}$$

where,

$$\Upsilon_1(t) = \frac{\beta_1\varpi}{2}\int_0^l \dot{\mu}^2 + \dot{\nu}^2 + \dot{\omega}^2 dr + \frac{\beta_1 T}{2}\int_0^l [\mu']^2 + [\nu']^2 dr + \frac{\beta_1 EA}{2}\int_0^l \Big(\omega' + \frac{[\mu']^2}{2} + \frac{[\nu']^2}{2}\Big)^2 dr, \tag{35}$$

$$\Upsilon_2(t) = \frac{\beta_1 M_p}{2}[\zeta_x^2(t) + \delta_x^2(t)] + \frac{1}{2\psi_x}\tilde{\bar{D}}_x^2(t) + \frac{\beta_1 M_p}{2}[\zeta_y^2(t) + \delta_y^2(t)] + \frac{1}{2\psi_y}\tilde{\bar{D}}_y^2(t) + \frac{\beta_1 M_p}{2}[\zeta_z^2(t) + \delta_z^2(t)] + \frac{1}{2\psi_z}\tilde{\bar{D}}_z^2(t), \tag{36}$$

$$\Upsilon_3(t) = \beta_2\varpi\int_0^l r[\dot{\mu}\mu' + \dot{\nu}\nu' + \dot{\omega}\omega']dr, \tag{37}$$

where $\tilde{\bar{D}}_k(t) = \bar{D}_k - \hat{\bar{D}}_k(t)$, $k = x, y, z$, and $\beta_1 > 0$ and $\beta_2 > 0$ are constants that satisfy $\beta_2\varpi l < \Gamma_1$ with the detailed form of Γ_1 given below in (42).

Next, we verify the positive definiteness of the Lyapunov candidate function (34). First, Equation (35) can be represented as:

$$\begin{aligned}\Upsilon_1(t) &= \frac{\beta_1\varpi}{2}\int_0^l \dot{\mu}^2 + \dot{\nu}^2 + \dot{\omega}^2 dr + \frac{\beta_1 T}{2}\int_0^l [\mu'\nu']^2 dr + \frac{\beta_1 EA}{2}\int_0^l \Big(\omega' + \frac{[\mu']^2}{2} + \frac{[\nu']^2}{2}\Big)^2 dr \\ &= \frac{\beta_1\varpi}{2}\int_0^l \dot{\mu}^2 + \dot{\nu}^2 + \dot{\omega}^2 dr + \frac{\beta_1 T}{2}\int_0^l [\mu'\nu']^2 dr + \frac{\beta_1 EA}{4}\int_0^l [\mu'\nu']^2 dr + \frac{\beta_1 EA}{8}\int_0^l [\mu']^4 dr \\ &\quad + \frac{\beta_1 EA}{8}\int_0^l [\nu']^4 dr + \frac{\beta_1 EA}{2}\int_0^l \omega'[\mu']^2 dr + \frac{\beta_1 EA}{2}\int_0^l \omega'[\nu']^2 dr + \frac{\beta_1 EA}{2}\int_0^l [\omega']^2 dr.\end{aligned} \tag{38}$$

According to [41], $2[\omega']^2 \le [\mu']^2$ and $2[\omega']^2 \le [\nu']^2$. By invoking Lemma 1, the cross terms in (38) satisfy the following inequalities:

$$-\frac{1}{2\varsigma_1}\int_0^l [\mu']^2 dr - \varsigma_1\int_0^l [\mu']^4 dr \le \int_0^l \omega'[\mu']^2 dr \le \frac{1}{2\varsigma_1}\int_0^l [\mu']^2 dr + \varsigma_1\int_0^l [\mu']^4 dr \tag{39}$$

and

$$-\frac{1}{2\varsigma_1}\int_0^l [\nu']^2 dr - \varsigma_1\int_0^l [\nu']^4 dr \le \int_0^l \omega'[\nu']^2 dr \le \frac{1}{2\varsigma_1}\int_0^l [\nu']^2 dr + \varsigma_1\int_0^l [\nu']^4 dr \tag{40}$$

where ς_1 denotes a positive constant satisfying $\frac{EA}{2T} \le \varsigma_1 \le \frac{1}{4}$. Then, we have:

$$\begin{aligned}&\frac{\beta_1\varpi}{2}\int_0^l \dot{\mu}^2 + \dot{\nu}^2 + \dot{\omega}^2 dr + \frac{\beta_1}{2}\Big(T - \frac{EA}{2\varsigma_1}\Big)\int_0^l [\mu']^2 + [\nu']^2 dr + \frac{\beta_1 EA}{2}\Big(\frac{1}{4} - \varsigma_1\Big)\int_0^l [\mu']^4 + [\nu']^4 dr \\ &+ \frac{\beta_1 EA}{4}\int_0^l [\mu'\nu']^2 dr + \frac{\beta_1 EA}{2}\int_0^l [\omega']^2 dr \\ \le\ & \Upsilon_1(t) \\ \le\ & \frac{\beta_1\varpi}{2}\int_0^l \dot{\mu}^2 + \dot{\nu}^2 + \dot{\omega}^2 dr + \frac{\beta_1}{2}\Big(T + \frac{EA}{2\varsigma_1}\Big)\int_0^l [\mu']^2 + [\nu']^2 dr + \frac{\beta_1 EA}{2}\Big(\frac{1}{4} + \varsigma_1\Big)\int_0^l [\mu']^4 + [\nu']^4 dr \\ &+ \frac{\beta_1 EA}{4}\int_0^l [\mu'\nu']^2 dr + \frac{\beta_1 EA}{2}\int_0^l [\omega']^2 dr.\end{aligned} \tag{41}$$

Furthermore, function $\Upsilon_1(t)$ satisfies the following inequation:

$$\Gamma_1\int_0^l \Pi(r,t)dr \le \Upsilon_1(t) \le \Gamma_2\int_0^l \Pi(r,t)dr, \tag{42}$$

where $\Pi(r,t) = \dot{\mu}^2 + \dot{\nu}^2 + \dot{\omega}^2 + [\mu']^2 + [\nu']^2 + [\omega']^2 + [\mu'\nu']^2 + [\mu']^4 + [\nu']^4$, $\Gamma_1 = \frac{\beta_1}{2}\min\{\varpi, T - \frac{EA}{2\varsigma_1}, EA(1/4 - \varsigma_1), EA\}$, and $\Gamma_2 = \frac{\beta_1}{2}\min\{\varpi, T + \frac{EA}{2\varsigma_1}, EA(1/4 + \varsigma_1), EA\}$.

In addition, by invoking $\o_1\o_2 \le \frac{\o_1^2}{2} + \frac{\o_2^2}{2}$, function $\Upsilon_3(t)$ satisfies the following relation:

$$|\Upsilon_3(t)| \le \frac{\beta_2\varpi l}{2}\int_0^l \dot{\mu}^2 + \dot{\nu}^2 + \dot{\omega}^2 + [\mu']^2 + [\nu']^2 + [\omega']^2 dr. \tag{43}$$

Then, we have:

$$|\Upsilon_3(t)| \le \frac{\beta_2\varpi l}{2}\int_0^l \Pi(r,t)dr. \tag{44}$$

From (42) and (44), we have that:

$$(\Gamma_1 - \beta_2\varpi l)\int_0^l \Pi(r,t)dr \le \Upsilon_1(t) + \Upsilon_3(t) \le (\Gamma_2 + \beta_2\varpi l)\int_0^l \Pi(r,t)dr. \tag{45}$$

By quoting (36), (45), and $\beta_2\varpi l < \Gamma_1$, we obtain:

$$c_1\Big(\int_0^l \Pi(r,t)dr + \Upsilon_2(t)\Big) \le \Upsilon(t) \le c_2\Big(\int_0^l \Pi(r,t)dr + \Upsilon_2(t)\Big), \quad (46)$$

where $c_1 = \min\{(\Gamma_1 - \beta_2\varpi l), 1\}$ and $c_2 = \max\{(\Gamma_2 + \beta_2\varpi l), 1\}$. Thus, function (34) can be selected as a Lyapunov candidate function.

In the following section, the stability of the three-dimensional HFSLS is proceeded under the Lyapunov candidate function (34).

Considering (8)-(11) and (35), the derivative of $\Upsilon_1(t)$ can be written as:

$$\begin{aligned}
&\dot{\Upsilon}_1(t)\\
=\;& \beta_1\varpi\int_0^l \dot{\mu}\ddot{\mu} + \dot{\nu}\ddot{\nu} + \dot{\omega}\ddot{\omega}dr + \beta_1 T\int_0^l \mu'\dot{\mu}' + \nu'\dot{\nu}'dr\\
&+\beta_1 EA\int_0^l \Big(\omega' + \frac{[\mu']^2}{2} + \frac{[\nu']^2}{2}\Big)\Big(\dot{\omega}' + \mu'\dot{\mu}' + \nu'\dot{\nu}'\Big)dr\\
=\;& \beta_1\int_0^l \dot{\mu}\Big\{T\mu'' + \frac{3EA}{2}[\mu']^2\mu'' + EA\Big(\mu'\omega'' + \mu''\omega'\Big)\\
&+\frac{EA}{2}\Big(\mu''[\nu']^2 + 2\mu'\nu'\nu''\Big) + u_{dx}\Big\} + \dot{\nu}\Big\{T\nu''\\
&+\frac{3EA}{2}[\nu']^2\nu'' + EA\Big(\nu'\omega'' + \nu''\omega'\Big) + \frac{EA}{2}\Big(\nu''[\mu']^2\\
&+2\mu'\mu''\nu'\Big) + u_{dy}\Big\} + \dot{\omega}\Big\{EA\omega'' + EA\mu'\mu''\\
&+EA\nu'\nu'' + u_{dz}\Big\}dr + \beta_1 T\int_0^l \mu'\dot{\mu}' + \nu'\dot{\nu}'dr\\
&+\beta_1 EA\int_0^l \Big(\omega' + \frac{[\mu']^2}{2} + \frac{[\nu']^2}{2}\Big)\Big(\dot{\omega}' + \mu'\dot{\mu}' + \nu'\dot{\nu}'\Big)dr\\
\le\;& \beta_1\dot{\mu}_l\Big\{EA\mu_l'\omega_l' + \frac{EA}{2}\mu_l'[\nu_l']^2 + \frac{EA}{2}[\mu_l']^3 + T\mu_l'\Big\}\\
&+\beta_1\dot{\nu}_l\Big\{EA\nu_l'\omega_l' + \frac{EA}{2}[\mu_l']^2\nu_l' + \frac{EA}{2}[\nu_l']^3 + T\nu_l'\Big\}\\
&+\beta_1\dot{\omega}_l\Big\{EA\omega_l' + \frac{EA}{2}[\mu_l']^2 + \frac{EA}{2}[\nu_l']^2\Big\}\\
&+\frac{\beta_1}{\varsigma_2}\int_0^l \dot{\mu}^2dr + \beta_1\varsigma_2\int_0^l u_{dx}^2dr + \frac{\beta_1}{\varsigma_3}\int_0^l \dot{\nu}^2dr\\
&+\beta_1\varsigma_3\int_0^l u_{dy}^2dr + \frac{\beta_1}{\varsigma_4}\int_0^l \dot{\omega}^2dr + \beta_1\varsigma_4\int_0^l u_{dz}^2dr\\
=\;& \beta_1\dot{\mu}_l\Big\{EA\mu_l'\omega_l' + \frac{EA}{2}\mu_l'[\nu_l']^2 + \frac{EA}{2}[\mu_l']^3\Big\}\\
&+\beta_1 T\Big\{\frac{\zeta_x^2(t)}{2} - \frac{\dot{\mu}_l^2}{2} - \frac{[\mu_l']^2}{2} - \frac{\delta_x^2(t)}{2} - \dot{\mu}_l\delta_x(t)\\
&-\mu_l'\delta_x(t)\Big\} + \beta_1\dot{\nu}_l\Big\{EA\nu_l'\omega_l' + \frac{EA}{2}[\mu_l']^2\nu_l' + \frac{EA}{2}\\
&\times[\nu_l']^3\Big\} + \beta_1 T\Big\{\frac{\zeta_y^2(t)}{2} - \frac{\dot{\nu}_l^2}{2} - \frac{[\nu_l']^2}{2} - \frac{\delta_y^2(t)}{2}\\
&-\dot{\nu}_l\delta_y(t) - \nu_l'\delta_y(t)\Big\} + \beta_1\dot{\omega}_l\Big\{\frac{EA}{2}[\mu_l']^2 + \frac{EA}{2}\\
&\times[\nu_l']^2\Big\} + \beta_1 EA\Big\{\frac{\zeta_z^2(t)}{2} - \frac{\dot{\omega}_l^2}{2} - \frac{[\omega_l']^2}{2} - \frac{\delta_z^2(t)}{2}\\
&-\dot{\omega}_l\delta_z(t) - \omega_l'\delta_z(t)\Big\} + \frac{\beta_1}{\varsigma_2}\int_0^l \dot{\mu}^2dr + \beta_1\varsigma_2 l\bar{u}_x^2 + \frac{\beta_1}{\varsigma_3}\\
&\times\int_0^l \dot{\nu}^2dr + \beta_1\varsigma_3 l\bar{u}_y^2 + \frac{\beta_1}{\varsigma_4}\int_0^l \dot{\omega}^2dr + \beta_1\varsigma_4 l\bar{u}_z^2, \quad (47)
\end{aligned}$$

where $\varsigma_2 - \varsigma_4 > 0$ denote constants.

By avoiding (12)-(14), (19)-(21), (25)-(33), and (36), and $|\zeta_k(t)| - \tanh\left(\frac{\zeta_k(t)}{\sigma_k}\right) \le 0.2785\sigma_k$ [24]. where, $k = x, y, z$ and the derivative of $\Upsilon_2(t)$ can be expressed as:

$$\begin{aligned}
&\dot{\Upsilon}_2(t)\\
=\;& \beta_1 M_p[\zeta_x(t)\dot{\zeta}_x(t) + \delta_x(t)\dot{\delta}_x(t)] + \tilde{\bar{D}}_x(t)\dot{\tilde{\bar{D}}}_x(t)\\
&+\beta_1 M_p[\zeta_y(t)\dot{\zeta}_y(t) + \delta_y(t)\dot{\delta}_y(t)] + \tilde{\bar{D}}_y(t)\dot{\tilde{\bar{D}}}_y(t)\\
&+\beta_1 M_p[\zeta_z(t)\dot{\zeta}_z(t) + \delta_z(t)\dot{\delta}_z(t)] + \tilde{\bar{D}}_z(t)\dot{\tilde{\bar{D}}}_z(t)\\
=\;& \beta_1\zeta_x(t)\Big\{\vartheta_x(t) + d_x(t) + M_p\dot{\mu}_l' - \gamma_x\delta_x(t) + T\dot{\mu}_l\Big\}\\
&+\beta_1\delta_x(t)\Big\{-\gamma_x\delta_x(t) + \Delta u_x(t) + T\mu_l' + T\dot{\mu}_l\\
&+\frac{EA}{2}[\mu_l']^3 + EA\mu_l'\omega_l' + \frac{EA}{2}\mu_l'[\nu_l']^2\Big\} + \psi_x\tilde{\bar{D}}_x(t)\\
&\times\Big\{-\beta_1\zeta_x(t)\tanh\Big(\frac{\zeta_x(t)}{\sigma_x}\Big) + \lambda_x\Big(\bar{D}_x - \tilde{\bar{D}}_x(t)\Big)\Big\}\\
&+\beta_1\zeta_y(t)\Big\{\vartheta_y(t) + d_y(t) + M_p\dot{\nu}_l' - \gamma_y\delta_y(t) + T\dot{\nu}_l\Big\}\\
&+\beta_1\delta_y(t)\Big\{-\gamma_y\delta_y(t) + \Delta u_y(t) + T\nu_l' + T\dot{\nu}_l\\
&+\frac{EA}{2}[\nu_l']^3 + EA\nu_l'\omega_l' + \frac{EA}{2}\nu_l'[\mu_l']^2\Big\} + \psi_y\tilde{\bar{D}}_y(t)\\
&\times\Big\{-\beta_1\zeta_y(t)\tanh\Big(\frac{\zeta_y(t)}{\sigma_y}\Big) + \lambda_y\Big(\bar{D}_y - \tilde{\bar{D}}_y(t)\Big)\Big\}\\
&+\beta_1\zeta_z(t)\Big\{\vartheta_z(t) + d_z(t) + M_p\dot{\omega}_l' - \gamma_z\delta_z(t)\Big\}\\
&+\beta_1\delta_z(t)\Big\{-\gamma_z\delta_z(t) + \Delta u_z(t) + EA\omega_l' + \frac{EA}{2}[\mu_l']^2\\
&+\frac{EA}{2}[\nu_l']^2\Big\} + \psi_z\tilde{\bar{D}}_z(t)\Big\{-\beta_1\zeta_z(t)\tanh\Big(\frac{\zeta_z(t)}{\sigma_z}\Big)\\
&+\lambda_z\Big(\bar{D}_z - \tilde{\bar{D}}_z(t)\Big)\Big\}\\
\le\;& -\beta_1 g_x\zeta_x^2(t) - \beta_1\zeta_x(t)\Big\{\frac{EA}{2}[\mu_l']^3 + EA\mu_l'\omega_l'\\
&+\frac{EA}{2}\mu_l'[\nu_l']^2\Big\} - \lambda_x\Big(1 - \frac{1}{\varsigma_5}\Big)\tilde{\bar{D}}_x^2(t) + \lambda_x\varsigma_5\bar{D}_x^2\\
&+0.2785\beta_1\sigma_x\bar{D}_x + \beta_1\zeta_x(t)\tanh\Big(\frac{\zeta_x(t)}{\sigma_x}\Big)\tilde{\bar{D}}_x(t)\\
&+\beta_1\delta_x(t)\Big\{-\gamma_x\delta_x(t) + T\mu_l' + T\dot{\mu}_l + \frac{EA}{2}[\mu_l']^3\\
&+EA\mu_l'\omega_l' + \frac{EA}{2}\mu_l'[\nu_l']^2\Big\} + \beta_1\frac{\delta_x^2(t)}{\varsigma_6} + \beta_1\varsigma_6\varepsilon_x^2\\
&-\beta_1 g_y\zeta_y^2(t) - \beta_1\zeta_y(t)\Big\{\frac{EA}{2}[\nu_l']^3 + EA\nu_l'\omega_l'\\
&+\frac{EA}{2}\nu_l'[\mu_l']^2\Big\} - \lambda_y\Big(1 - \frac{1}{\varsigma_7}\Big)\tilde{\bar{D}}_y^2(t) + \lambda_y\varsigma_7\bar{D}_y^2\\
&+0.2785\beta_1\sigma_y\bar{D}_y + \beta_1\zeta_y(t)\tanh\Big(\frac{\zeta_y(t)}{\sigma_y}\Big)\tilde{\bar{D}}_y(t)\\
&+\beta_1\delta_y(t)\Big\{-\gamma_y\delta_y(t) + T\nu_l' + T\dot{\nu}_l + \frac{EA}{2}[\nu_l']^3\\
&+EA\nu_l'\omega_l' + \frac{EA}{2}\nu_l'[\mu_l']^2\Big\} + \beta_1\frac{\delta_y^2(t)}{\varsigma_8} + \beta_1\varsigma_8\varepsilon_y^2\\
&-\beta_1 g_z\zeta_z^2(t) + \beta_1\zeta_z(t)\Big\{EA\omega_l' + \frac{EA}{2}[\mu_l']^2
\end{aligned}$$

$$+\frac{EA}{2}[\nu_l']^2\Big\} - \lambda_z\Big(1-\frac{1}{\varsigma_9}\Big)\tilde{\tilde{D}}_z^2(t) + \lambda_z\varsigma_9\bar{D}_z^2$$
$$+0.2785\beta_1\sigma_z\bar{D}_z + \beta_1\zeta_z(t)\tanh\Big(\frac{\zeta_z(t)}{\sigma_z}\Big)\tilde{\tilde{D}}_z(t)$$
$$+\beta_1\delta_z(t)\Big\{-\gamma_z\delta_z(t) + EA\omega_l' + \frac{EA}{2}[\mu_l']^2$$
$$+\frac{EA}{2}[\nu_l']^2\Big\} + \beta_1\frac{\delta_z^2(t)}{\varsigma_{10}} + \beta_1\varsigma_{10}\varepsilon_z^2, \tag{48}$$

where $\varsigma_5 - \varsigma_{10} > 0$ denote constants.

By quoting (8)-(11) and (37), we calculate the derivative of $\Upsilon_3(t)$ as follows:

$$\begin{aligned}
&\dot{\Upsilon}_3(t)\\
=\;& \beta_2\varpi\int_0^l r[\ddot{\mu}\mu' + \dot{\mu}\dot{\mu}' + \ddot{\nu}\nu' + \dot{\nu}\dot{\nu}' + \ddot{\omega}\omega' + \dot{\omega}\dot{\omega}']dr\\
=\;& \beta_2\int_0^l r\mu'\Big\{T\mu'' + \frac{3EA}{2}[\mu']^2\mu'' + EA[\mu'\omega'' + \mu''\omega']\\
&+\frac{EA}{2}\Big(\mu''[\nu']^2 + 2\mu'\nu'\nu''\Big) + u_{dx}\Big\} + r\nu'\Big\{T\nu''\\
&+\frac{3EA}{2}[\nu']^2\nu'' + EA[\nu'\omega'' + \nu''\omega'] + \frac{EA}{2}\Big(\nu''[\mu']^2\\
&+2\mu'\mu''\nu'\Big) + u_{dy}\Big\} + r\omega'\Big\{EA\omega'' + EA\mu'\mu''\\
&+EA\nu'\nu'' + u_{dz}\Big\} + r\dot{\mu}\dot{\mu}' + r\dot{\nu}\dot{\nu}' + r\dot{\omega}\dot{\omega}'dr\\
\leq\;& -\frac{\beta_2\varpi}{2}\int_0^l \dot{\mu}^2 + \dot{\nu}^2 + \dot{\omega}^2dr - \beta_2\Big(\frac{T}{2} - \frac{EA}{\varsigma_{11}} - \frac{l}{\varsigma_{13}}\Big)\\
&\times\int_0^l[\mu']^2dr - \beta_2\Big(\frac{T}{2} - \frac{EA}{2\varsigma_{12}} - \frac{l}{\varsigma_{14}}\Big)\int_0^l[\nu']^2dr\\
&-\beta_2\Big(\frac{EA}{2} - \frac{l}{\varsigma_{14}}\Big)\int_0^l[\omega']^2dr - \beta_2EA\Big(\frac{3l}{8} - \varsigma_{11}\Big)\\
&\times\int_0^l[\mu']^4dr - \beta_2EA\Big(\frac{3l}{8} - \varsigma_{12}\Big)\int_0^l[\nu']^4dr - \frac{3\beta_2}{4}\\
&\times EA\int_0^l[\mu'\nu']^2dr + \frac{\beta_2 l}{2}\varpi[\dot{\mu}_l^2 + \dot{\nu}_l^2 + \dot{\omega}_l^2] + \frac{\beta_2 lT}{2}\\
&\times\Big([\mu_l']^2 + [\nu_l']^2\Big) + \frac{\beta_2 l}{2}EA[\omega_l']^2 + \frac{3\beta_2 lEA}{8}\Big([\mu_l']^4\\
&+[\nu_l']^4\Big) + \beta_2EAl\Big([\mu_l']^2 + [\nu_l']^2\Big)\omega_l' + \frac{3\beta_2}{4}EAl[\mu_l\nu_l]^2\\
&+\beta_2 l^2\Big(\varsigma_{13}\bar{u}_x^2 + \varsigma_{14}\bar{u}_y^2 + \varsigma_{15}\bar{u}_z^2\Big),
\end{aligned}\tag{49}$$

where $\varsigma_{11} - \varsigma_{15} > 0$ denote constants.

Synthesizing the above results in (47)-(49) and considering $2[\omega']^2 \leq [\mu']^2$ and $2[\omega']^2 \leq [\nu']^2$, the derivative of $\Upsilon(t)$ can be written as:

$$\begin{aligned}
&\dot{\Upsilon}(t) = \dot{\Upsilon}_1(t) + \dot{\Upsilon}_2(t) + \dot{\Upsilon}_3(t)\\
\leq\;& -\Big(\frac{\beta_2\varpi}{2} - \frac{\beta_1}{\varsigma_2}\Big)\int_0^l\dot{\mu}^2dr - \Big(\frac{\beta_2\varpi}{2} - \frac{\beta_1}{\varsigma_3}\Big)\int_0^l\dot{\nu}^2dr\\
&-\Big(\frac{\beta_2\varpi}{2} - \frac{\beta_1}{\varsigma_4}\Big)\int_0^l\dot{\omega}^2dr - \beta_2\Big(\frac{T}{2} - \frac{EA}{2\varsigma_8} - \frac{l}{\varsigma_{13}}\Big)\\
&\times\int_0^l[\mu']^2dr - \beta_2\Big(\frac{T}{2} - \frac{EA}{2\varsigma_{12}} - \frac{l}{\varsigma_{14}}\Big)\int_0^l[\nu']^2dr\\
&-\beta_2\Big(\frac{EA}{2} - \frac{l}{\varsigma_{15}}\Big)\int_0^l[\omega']^2dr - \beta_2EA\Big(\frac{3l}{8} - \varsigma_{11}\Big)\\
&\times\int_0^l[\mu']^4dr - \beta_2EA\Big(\frac{3l}{8} - \varsigma_{12}\Big)\int_0^l[\nu']^4dr - \frac{3\beta_2EA}{4}\\
&\times\int_0^l[\mu'\nu']^2dr - \beta_1\Big(g_x - \frac{T}{2}\Big)\zeta_x^2(t) - \beta_1\Big(\gamma_x + \frac{T}{2}\\
&-\frac{1}{\varsigma_6}\Big)\delta_x^2(t) - \beta_1\Big(g_y - \frac{T}{2}\Big)\zeta_y^2(t) - \beta_1\Big(\gamma_y + \frac{T}{2} - \frac{1}{\varsigma_8}\Big)\\
&\times\delta_y^2(t) - \beta_1\Big(g_z - \frac{EA}{2}\Big)\zeta_z^2(t) - \beta_1\Big(\gamma_z + \frac{EA}{2} - \frac{1}{\varsigma_{10}}\\
&-EA\varsigma_{16}\Big)\delta_z^2(t) - \lambda_x\Big(1 - \frac{1}{\varsigma_5}\Big)\tilde{\tilde{D}}_x^2(t) - \lambda_y\Big(1 - \frac{1}{\varsigma_7}\Big)\\
&\times\tilde{\tilde{D}}_y^2(t) - \lambda_z\Big(1 - \frac{1}{\varsigma_9}\Big)\tilde{\tilde{D}}_z^2(t) + (\beta_1\varsigma_2 l + \beta_2 l^2\varsigma_{13})\bar{u}_x^2\\
&+\lambda_x\varsigma_5\bar{D}_x^2 + 0.2785\beta_1\sigma_x\bar{D}_x + (\beta_1\varsigma_3 l + \beta_2 l^2\varsigma_{14})\bar{u}_y^2\\
&+\lambda_y\varsigma_7\bar{D}_y^2 + 0.2785\beta_1\sigma_y\bar{D}_y + (\beta_1\varsigma_4 l + \beta_2 l^2\varsigma_{15})\bar{u}_z^2\\
&+\lambda_z\varsigma_9\bar{D}_z^2 + 0.2785\beta_1\sigma_z\bar{D}_z\\
\leq\;& -\upsilon_1\Big(\int_0^l\Pi(r,t)dr + \Upsilon_2(t)\Big) + \upsilon_2\\
\leq\;& -\frac{\upsilon_1}{c_2}\Upsilon(t) + \upsilon_2,
\end{aligned}\tag{50}$$

where

$$\begin{aligned}
\upsilon_1 =\;& \min\Big\{\frac{\beta_2\varpi}{2} - \frac{\beta_1}{\varsigma_2}, \frac{\beta_2\varpi}{2} - \frac{\beta_1}{\varsigma_3}, \frac{\beta_2\varpi}{2} - \frac{\beta_1}{\varsigma_4},\\
&\beta_2\Big(\frac{T}{2} - \frac{EA}{2\varsigma_8} - \frac{l}{\varsigma_{13}}\Big), \beta_2\Big(\frac{T}{2} - \frac{EA}{2\varsigma_{12}} - \frac{l}{\varsigma_{14}}\Big),\\
&\beta_2\Big(\frac{EA}{2} - \frac{l}{\varsigma_{15}}\Big), \beta_2EA\Big(\frac{3l}{8} - \varsigma_{11}\Big), \frac{3\beta_2EA}{4},\\
&\beta_2EA\Big(\frac{3l}{8} - \varsigma_{12}\Big), \frac{2g_x - T}{M_p}, \frac{2\gamma_x + T - \frac{2}{\varsigma_6}}{M_p},\\
&\frac{2g_y - T}{M_p}, \frac{2\gamma_y + T - \frac{2}{\varsigma_8}}{M_p}, \frac{2g_z - EA}{M_p},\\
&\frac{2\gamma_z + EA - 2EA\varsigma_{16} - \frac{2}{\varsigma_{10}}}{M_p}, 2\lambda_x\psi_x\Big(1 - \frac{1}{\varsigma_5}\Big),\\
&2\lambda_y\psi_y\Big(1 - \frac{1}{\varsigma_7}\Big), 2\lambda_z\psi_z\Big(1 - \frac{1}{\varsigma_9}\Big)\Big\},\\
\upsilon_2 =\;& (\beta_1\varsigma_2 l + \beta_2 l^2\varsigma_{13})\bar{u}_x^2 + \lambda_x\varsigma_5\bar{D}_x^2 + 0.2785\beta_1\sigma_x\bar{D}_x\\
&+(\beta_1\varsigma_3 l + \beta_2 l^2\varsigma_{14})\bar{u}_y^2 + \lambda_y\varsigma_7\bar{D}_y^2 + 0.2785\beta_1\sigma_y\bar{D}_y\\
&+(\beta_1\varsigma_4 l + \beta_2 l^2\varsigma_{15})\bar{u}_z^2 + \lambda_z\varsigma_9\bar{D}_z^2 + 0.2785\beta_1\sigma_z\bar{D}_z,
\end{aligned}$$

under

$$\begin{aligned}
&\beta_1T - \beta_2 l\varpi \geq 0, \frac{\beta_1EA}{2} - \frac{\beta_1EA}{\varsigma_{16}} - \frac{\beta_2 l\varpi}{2} \geq 0,\\
&\beta_1T - \beta_2 lT - \frac{|\beta_2 l - 3/2\beta_1|EA}{\varsigma_{17}} \geq 0,\\
&\beta_1T - \beta_2 lT - \frac{|\beta_2 l - 3/2\beta_1|EA}{\varsigma_{18}} \geq 0,\\
&\beta_1EA - \beta_2 lEA \geq 0, \beta_1EA - \frac{3\beta_1 lEA}{4} \geq 0,\\
&\frac{\beta_1EA}{2} - \frac{3\beta_2 lEA}{8} - \varsigma_{17}|\beta_2 l - 3/2\beta_1|EA \geq 0,\\
&\frac{\beta_1EA}{2} - \frac{3\beta_2 lEA}{8} - \varsigma_{18}|\beta_2 l - 3/2\beta_1|EA \geq 0,
\end{aligned}$$

with $\varsigma_{16} - \varsigma_{18} > 0$ being constants.

According to the above analysis and [42], the closed-loop system of the three-dimensional HFSLS is confirmed to be semi-uniformly bounded. The convergence of the vibration values $\mu(r,t)$, $\nu(r,t)$, $\omega(r,t)$, and $r\in[0,l]$ for the three-dimensional HFSLS are analyzed in the theorem as follows.

Theorem 1: Consider a three-dimensional HFSLS subject to input saturation and backlash described by (8)-(14) with unbounded initial values and the adaptive boundary control scheme given by (28)-(33), the vibration values $\mu(r,t)$, $\nu(r,t)$, $\omega(r,t)$, and $r\in[0,l]$ proved to be semi-uniformly ultimately bounded.

Proof: Letting $\upsilon_3=\frac{\upsilon_1}{c_2}$, we obtain that $\dot{\Upsilon}(t)\le-\upsilon_3\Upsilon(t)+\upsilon_2$. The above inequality (50) is calculated as follows:

$$\Upsilon(t)\le\Upsilon(0)\exp(-\upsilon_3 t)+\frac{\upsilon_2}{\upsilon_3}. \tag{51}$$

where $\Upsilon(0)$ is the initial value of function $\Upsilon(t)$. Invoking Lemma 1 and (46), it follows that:

$$\frac{\mu^2}{l}\le\int_0^l[\mu']^2dr\le\int_0^l\Pi(r,t)\le\frac{\Upsilon(t)}{\upsilon_1}, \tag{52}$$

$$\frac{\nu^2}{l}\le\int_0^l[\nu']^2dr\le\int_0^l\Pi(r,t)\le\frac{\Upsilon(t)}{\upsilon_1}, \tag{53}$$

$$\frac{\omega^2}{l}\le\int_0^l[\omega']^2dr\le\int_0^l\Pi(r,t)\le\frac{\Upsilon(t)}{\upsilon_1}. \tag{54}$$

Subsequently, by quoting (51), (52), (53), and (54), we have:

$$|\mu|\le\sqrt{\frac{l\Upsilon(0)\exp(-\upsilon_3 t)}{\upsilon_1}+\frac{\upsilon_2 l}{\upsilon_1\upsilon_3}}, \tag{55}$$

$$|\nu|\le\sqrt{\frac{l\Upsilon(0)\exp(-\upsilon_3 t)}{\upsilon_1}+\frac{\upsilon_2 l}{\upsilon_1\upsilon_3}}, \tag{56}$$

$$|\omega|\le\sqrt{\frac{l\Upsilon(0)\exp(-\upsilon_3 t)}{\upsilon_1}+\frac{\upsilon_2 l}{\upsilon_1\upsilon_3}}. \tag{57}$$

When $t\to+\infty$, it derives that:

$$|\mu|\le\sqrt{\frac{\upsilon_2 l}{\upsilon_3\upsilon_1}},\ |\nu|\le\sqrt{\frac{\upsilon_2 l}{\upsilon_3\upsilon_1}},\ |\omega|\le\sqrt{\frac{\upsilon_2 l}{\upsilon_3\upsilon_1}}. \tag{58}$$

Thus, the vibration values $\mu(r,t)$, $\nu(r,t)$, $\omega(r,t)$, and $r\in[0,l]$ of the three-dimensional HFSLS are proved to be semi-uniformly ultimately bounded. Furthermore, $|\mu|\le\sqrt{\frac{\upsilon_2 l}{\upsilon_3\upsilon_1}}$, $|\nu|\le\sqrt{\frac{\upsilon_2 l}{\upsilon_3\upsilon_1}}$, and $|\omega|\le\sqrt{\frac{\upsilon_2 l}{\upsilon_3\upsilon_1}}$.

IV. Numerical Simulation

Consider the three-dimensional HFSLS subject to input saturation and backlash, given by (8)-(14) and the system parameters below: $l=1.0$ m, $\varpi=0.1$ kg/m, $T=16$ N, $EA=1.2$ N, and $m_l=3.0$ kg. The boundary disturbances and distributed loads are as follows: $d_x(t)=(1.0+0.5\sin(0.5t)+0.3\sin(0.3t)+0.2\sin(0.2t))\times10$, $d_y(t)=(1.0+0.5\sin(0.5t)+0.3\sin(0.3t)+0.2\sin(0.2t))\times10$, $d_z(t)=(1.5+0.5\sin(0.5t)+0.3\sin(0.3t)+0.2\sin(0.2t))$, $u_{dx}=(1.0+0.4\sin(0.1\pi t)+0.2\sin(0.2\pi t)+0.1\sin(0.4\pi t))r/5$, $u_{dy}=(1.0+0.4\sin(0.1\pi t)+0.2\sin(0.2\pi t)+0.1\sin(0.4\pi t))r/5$, and $u_{dz}=(0.5+0.4\sin(0.1\pi t)+0.2\sin(0.2\pi t)+0.1\sin(0.4\pi t))r/10$. The backlash spacings are shown as: $\iota_{xr}=\iota_{yr}=4$, $\iota_{zr}=2$, $\iota_{xl}=\iota_{yl}=4$, and $\iota_{zl}=2$. The slop parameters of the backlash function are $\xi_x=\xi_y=\xi_z=1$ and the saturation levels are given by $\vartheta_{xM}=24$, $\vartheta_{xm}=-34$,and $\vartheta_{yM}=24$, $\vartheta_{ym}=-34$, $\vartheta_{zM}=12$, and $\vartheta_{xm}=-12$.

Here we discuss the stability of a three-dimensional HFSLS under two circumstances.

Circumstance I: Without control.

The response curves of the open-loop system of the three-dimensional HFSLS are shown in Fig. 3-8. Figs. 3-5 display the simulation curves $\mu(r,t)$, $\nu(r,t)$, and $\omega(r,t)$ for the three-dimensional HFSLS without control. When $r=l$, the corresponding curves $\mu(l,t)$, $\nu(l,t)$, and $\omega(l,t)$ are as shown in Figs. 6-8. According to Figs. 3-8, the swing amplitude of the slung-load system is large. Therefore, an efficient control strategy must be proposed to reduce vibration.

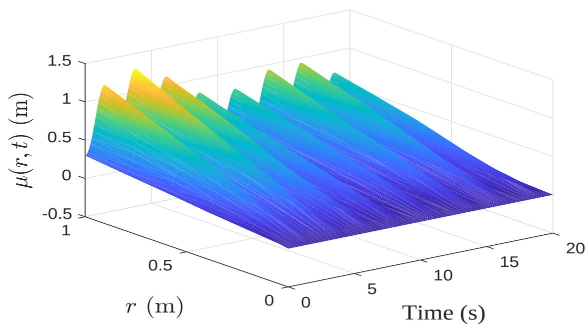

Fig. 3: The simulation curve of $\mu(r,t)$ without control.

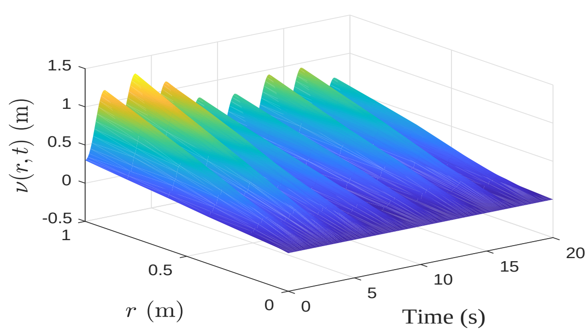

Fig. 4: The simulation curve of $\nu(r,t)$ without control.

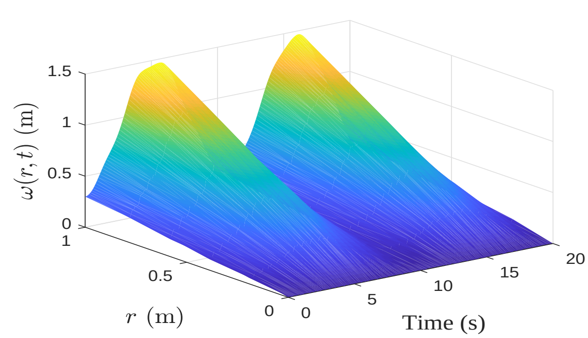

Fig. 5: The simulation curve of $\omega(r,t)$ without control.

Circumstance II: With control.

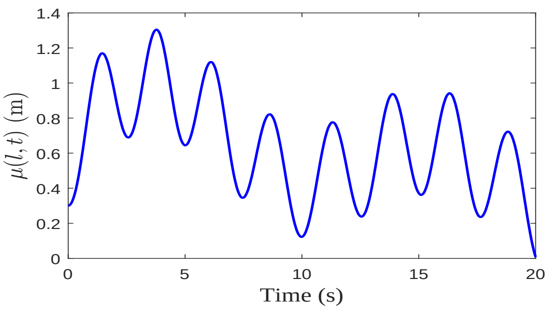

Fig. 6: The simulation curve of $\mu(l,t)$ without control.

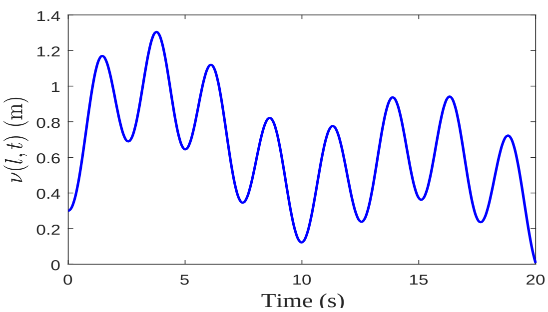

Fig. 7: The simulation curve of $\nu(l,t)$ without control.

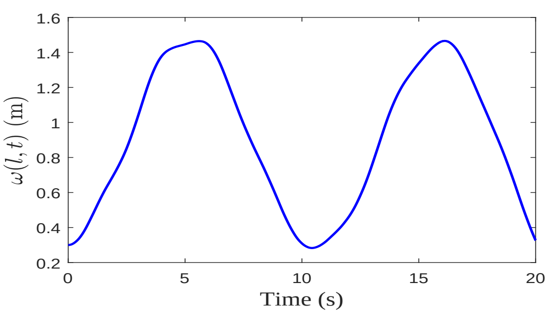

Fig. 8: The simulation curve of $\omega(l,t)$ without control.

The design parameters of the control scheme given by (28)-(33) are as follows: $\beta_1 = 1$, $\psi_x = \psi_y = \psi_z = 0.1$, $\lambda_x = \lambda_y = \lambda_z = 0.1$, $\sigma_x = \sigma_y = \sigma_z = 0.1$, $\gamma_x = \gamma_y = \gamma_z = 1.0 \times 10^2$, and $g_x = g_y = g_z = 1.0 \times 10^3$. Under the introduced control laws given by (28)-(33) the simulation curves $\mu(r,t)$, $\nu(r,t)$, and $\omega(r,t)$ of the closed-loop system of the three-dimensional HFSLS are shown in Figs. 9-11.

To verify the performance of the proposed control scheme, we developed the following PD control: $\vartheta_x = -\kappa_{px}\mu(l,t) - \kappa_{dx}\dot{\mu}(l,t)$, $\vartheta_y = -\kappa_{py}\nu(l,t) - \kappa_{dy}\dot{\nu}(l,t)$, and $\vartheta_z = -\kappa_{pz}\omega(l,t) - \kappa_{dz}\dot{\omega}(l,t)$ where $\kappa_{px} = \kappa_{py} = 300$, $\kappa_{dx} = \kappa_{dy} = 200$, $\kappa_{pz} = 100$, and $\kappa_{dz} = 200$. With the PD control, the simulation curves $\mu(r,t)$, $\nu(r,t)$, and $\omega(r,t)$ are shown in Figs. 12-14.

Comparing the simulation graphs of the vibration amplitudes $\mu(r,t)$, $\nu(r,t)$, and $\omega(r,t)$ at $r = l$ in Figs. 15-17, it is clear that the proposed control strategy has a better anti-vibration control performance than PD control. Figs. 18-20 show that the phenomena of input nonlinearities appear in the process of control design, which suggests that proposed control strategy effectively addresses input nonlinearities.

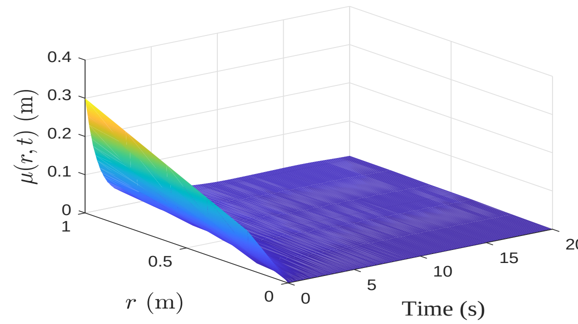

Fig. 9: The simulation curve of $\mu(r,t)$ with proposed control.

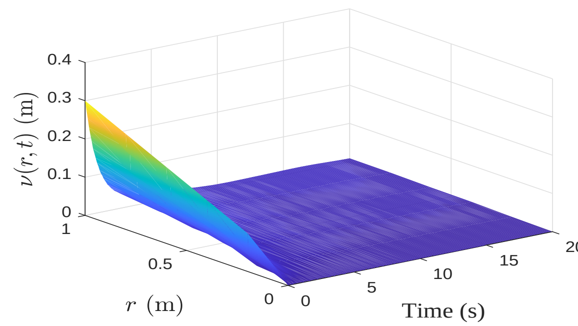

Fig. 10: The simulation curve of $\nu(r,t)$ with proposed control.

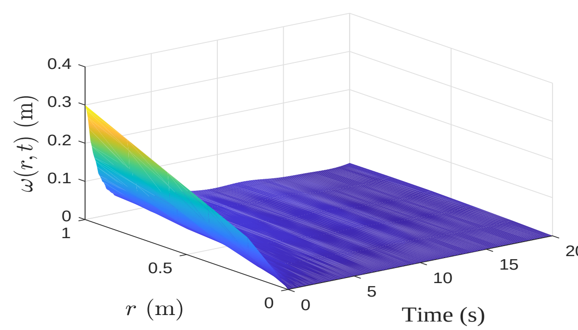

Fig. 11: The simulation curve of $\omega(r,t)$ with proposed control.

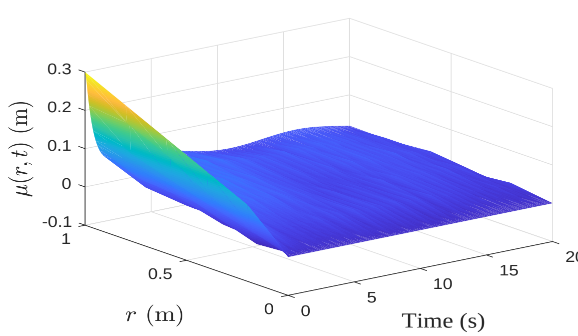

Fig. 12: The simulation curve of $\mu(r,t)$ with PD control.

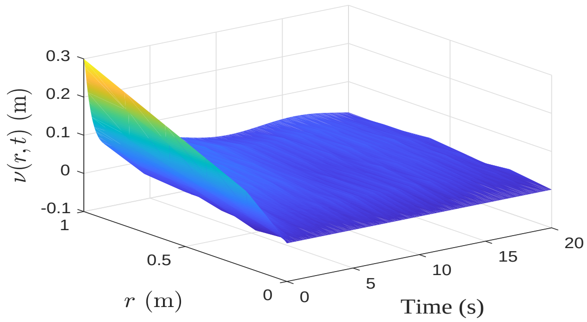

Fig. 13: The simulation curve of $\nu(r,t)$ with PD control.

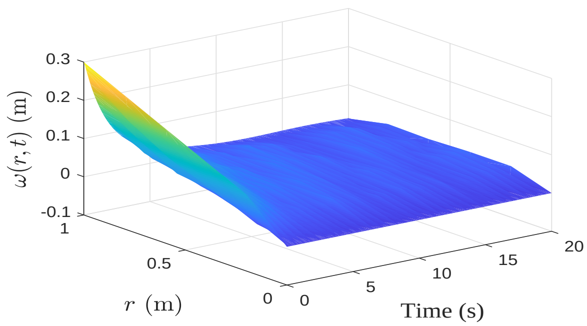

Fig. 14: The simulation curve of $\omega(r,t)$ with PD control.

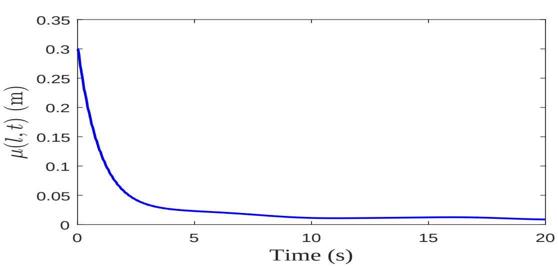

(a)

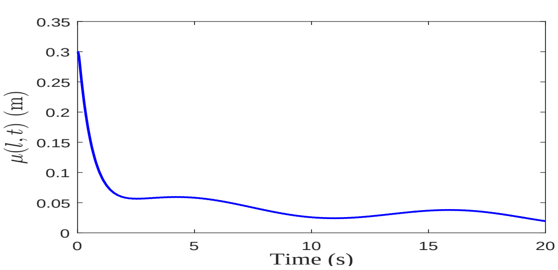

(b)

Fig. 15: (a) The simulation curve of $\mu(l,t)$ with proposed control; (b) The simulation curve of $\mu(l,t)$ with PD control.

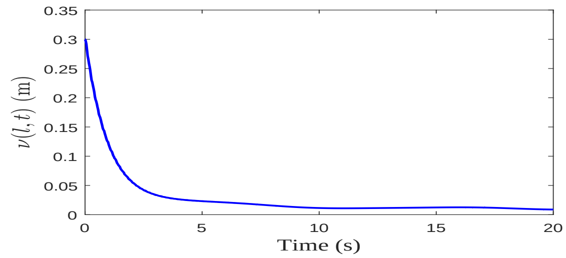

(a)

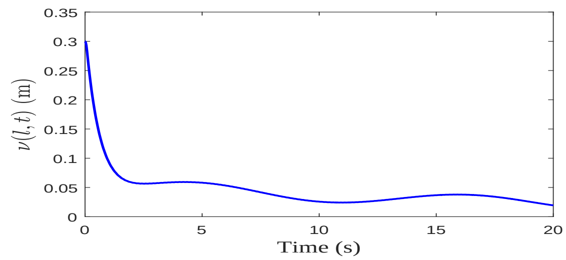

(b)

Fig. 16: (a) The simulation curve of $\nu(l,t)$ with proposed control; (b) The simulation curve of $\nu(l,t)$ with PD control.

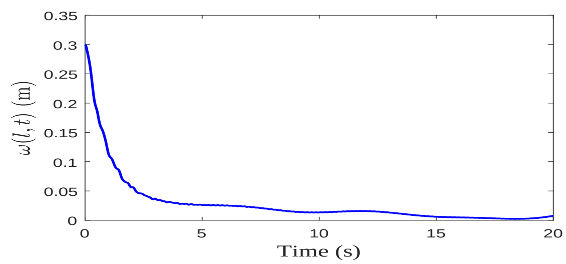

(a)

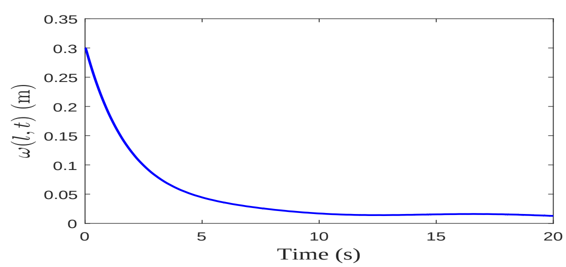

(b)

Fig. 17: (a) The simulation curve of $\omega(l,t)$ with proposed control; (b) The simulation curve of $\omega(l,t)$ with PD control.

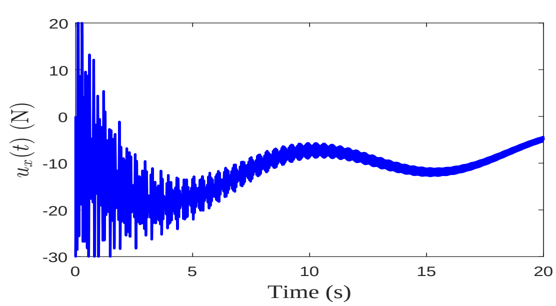

Fig. 18: The control input $u_x(t)$.

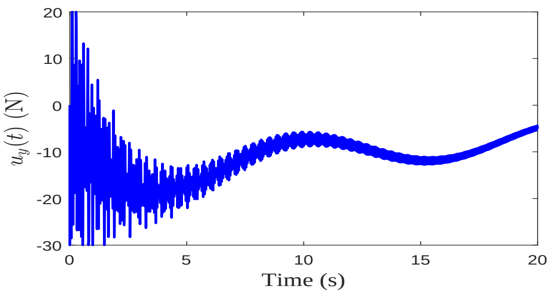

Fig. 19: The control input $u_y(t)$.

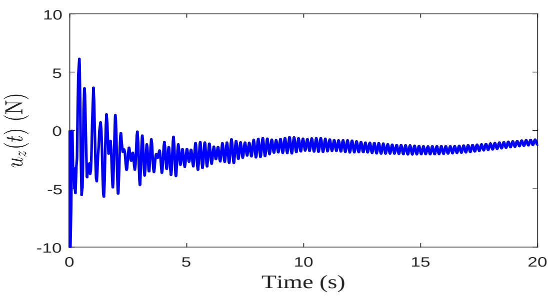

Fig. 20: The control input $u_z(t)$.

Based on the above discussion, the developed adaptive boundary control scheme enhances performance robustness against input saturation, input backlash, and external disturbances. Furthermore, it also allows for effective anti-vibration control of three-dimensional HFSLS.

V. Conclusion

In this study, a new three-dimensional HFSLS model was constructed using the extended Hamiltonian principle and an adaptive boundary-control method was developed to investigate the stabilization problem using the Lyapunov direct method. The proposed scheme has two attractive features: 1) The input saturation and input backlash are translated into a new saturation function, that can be disposed of by designing auxiliary systems. Thus, the number of calculations required to address saturation and backlash is reduced. 2) A novel adaptive boundary control was derived to guarantee the semi-uniform ultimate boundedness of a three-dimensional HFSLS with input saturation and backlash. A numerical simulation was conducted to demonstrate the control performance of the proposed control scheme. The prospective study includes a reinforcement learning approach [43], [44] and event-triggered mechanisms [45] for the three-dimensional HFSLS.

References

[1] M. Bisgaard, J. Bendtsen, and A. Cour-Harbo, "Modeling of generic slung load system," *Journal of Guidance Control and Dynamics*, vol. 32, no. 2, pp. 573-585, 2009.

[2] S. Yang and B. Xian, "Energy-based nonlinear adaptive control design for the quadrotor UAV system with a suspended payload," *IEEE Transactions on Industrial Electronics*, vol. 67, no. 3, pp. 2054-2064, 2020.

[3] B. Xian, S. Wang, and S. Yang, "Robust tracking control of a quadrotor unmanned aerial vehicle-suspended payload system," *IEEE/ASME Transactions on Mechatronics*, vol. 26, no. 5, pp. 2653-2663, 2021.

[4] W. Liu, M. Chen, and P. Shi, "Fixed-time disturbance observer-based control for quadcopter suspension transportation system," *IEEE Transactions on Circuits and Systems I-Regular Papers*, early access, 2022, doi: 10.1109/TCSI.2022.3193878.

[5] M. Chen, Y. Ren, and J. Liu, "Antidisturbance control for a suspension cable system of helicopter subject to input nonlinearities," *IEEE Transactions on Systems, Man, and Cybernetics: Systems*, vol. 48, no. 12, pp. 2292-2304, 2018.

[6] Y. Ren, M. Chen, and J. Liu, "Bilateral coordinate boundary adaptive control for a helicopter lifting system with backlash-like hysteresis," *SCIENCE CHINA Information Sciences*, vol. 63, no. 1, pp. 119203, 2020.

[7] Y. Ren, Z. Zhao, C. K. Ahn, and H.-X. Li, "Adaptive fuzzy control for an uncertain axially moving slung-load cable system of a hovering helicopter with actuator fault," *IEEE Transactions on Fuzzy Systems*, vol. 30, no. 11, pp. 4915-4925, 2022.

[8] W. He, H. Qin, and J.-K. Liu, "Modelling and vibration control for a flexible string system in three-dimensional space," *IET Control Theory and Applications*, vol. 9, no. 16, pp. 2387-2394, 2015.

[9] Y. Song, W. He, X. He, and Z. Han, "Vibration control of a high-rise building structure: Theory and experiment," *IEEE/CAA Journal Automatica Sinica*, vol. 8, no. 4, pp. 866-875, 2021.

[10] W. He, X. Mu, L. Zhang, and Y. Zou, "Modeling and trajectory tracking control for flapping-wing micro aerial vehicles," *IEEE/CAA Journal Automatica Sinica*, vol. 8, no. 1, pp. 148-156, 2021.

[11] Z. Liu, J. Liu, and W. He, "Modeling and vibration control of a flexible aerial refueling hose with variable lengths and input constraint," *Automatica*, vol. 77, pp. 302-310, 2017.

[12] Z. Liu, Z. Han, Z. Zhao, and W. He, "Modeling and adaptive control for a spatial flexible spacecraft with unknown actuator failures," *SCIENCE CHINA Information Sciences*, vol. 64, no. 5, pp. 152208, 2021.

[13] Z. Liu, J. Shi, Y. He, Z. Zhao, and H.-K. Lam, "Adaptive fuzzy control for a spatial flexible hose system with dynamic event-triggered mechanism," *IEEE Transactions on Aerospace and Electronic Systems*, early access, 2022, doi: 10.1109/TAES.2022.3197551.

[14] Y. Ren, Z. Zhao, C. Zhang, Q. Yang, and K.-S. Hong, "Adaptive neural-network boundary control for a flexible manipulator with input constraints and model uncertainties," *IEEE Transactions on Cybernetics*, vol. 51, no. 10, pp. 4796-4807, 2021.

[15] Y. Ren, P. Zhu, Z. Zhao, J. Yang, and T. Zou, "Adaptive fault-tolerant boundary control for a flexible string with unknown dead-zone and actuator fault," *IEEE Transactions on Cybernetics*, vol. 52, no. 7, pp. 7084-7093, 2022.

[16] Y. Liu, F. Guo, X. He, and Q. Hui, "Boundary control for an axially moving system with input restriction based on disturbance observers," *IEEE Transactions on Systems, Man and Cybernetics: Systems*, vol. 49, no. 11, pp. 2242-2253, 2019.

[17] Y. Liu, X. Chen, Y. Mei, and Y. Wu, "Observer-based boundary control for an asymmetric output-constrained flexible robotic manipulator," *SCIENCE CHINA Information Sciences*, vol. 65, no. 3, pp. 139203, 2022.

[18] Z. Zhao and Z. Liu, "Finite-time convergence disturbance rejection control for a flexible Timoshenko manipulator," *IEEE/CAA Journal Automatica Sinica*, vol. 8, no. 1, pp. 157-168, 2021.

[19] S. Chen, Z. Zhao, D. Zhu, C. Zhang, and H.-X. Li, "Adaptive robust control for a spatial flexible timoshenko manipulator subject to input dead-zone," *IEEE Transactions on Systems, Man, and Cybernetics: Systems*, vol. 52, no. 3, pp. 1395-1404, 2022.

[20] Z. Zhao, Z. Liu, W. He, K. Hong, and H.-X. Li, "Boundary adaptive fault-tolerant control for a flexible Timoshenko arm with backlash-like hysteresis," *Automatica*, vol. 130, pp. 109690, 2021.

[21] Z. Han, Z. Liu, W. Kang, and W. He, "Boundary feedback control of a nonhomogeneous wind turbine tower with exogenous disturbances," *IEEE Transactions on Automatic Control*, vol. 67, no. 4, pp. 1952-1959, 2022.

[22] Y. Liu, Y. Mei, H. Cai, C. He, T. Liu, and G. Hu, "Asymmetric input-output constraint control of a flexible variable-length rotary crane arm," *IEEE Transactions on Cybernetics*, vol. 52, no. 10, pp. 10582-10591, 2022.

[23] X. He, Y. Ma, M. Chen, and W. He, "Flight and vibration control of flexible air-breathing hypersonic vehicles under actuator faults," *IEEE Transactions on Cybernetics*, early access, 2022, doi: 10.1109/TCYB.2022.3140536.

[24] M. Chen, S. S. Ge, and B. B. Ren, "Adaptive tracking control of uncertain MIMO nonlinear systems with input constraints," *Automatica*, vol. 47, no. 3, pp. 452-465, 2011.

[25] L. Liu, Y.-J. Liu, A, Chen, S. Tong, and C. L. Philip Chen, "Integral barrier Lyapunov function based adaptive control for switched nonlinear systems," *SCIENCE CHINA Information Sciences*, vol. 63, no. 3, pp. 132203, 2020.

[26] L. Liu, T. Gao, Y.-J. Liu, S. Tong, and C. L. Philip Chen, “Time-varying IBLFs-based adaptive control of uncertain nonlinear systems with full state constraints,” *Automatica*, vol. 129, pp. 109595, 2021.
[27] J. Zhang, K. Li, and Y. Li, “Output-feedback based simplified optimized backstepping control for strict-feedback systems with input and state constraints,” *IEEE/CAA Journal Automatica Sinica*, vol. 8, no. 6, pp. 1119-1132, 2021.
[28] Z. Li and J. Zhao, “Adaptive consensus of non-strict feedback switched multi-agent systems with input saturations,” *IEEE/CAA Journal Automatica Sinica*, vol. 8, no. 11, pp. 1752-1761, 2021.
[29] Y. Yang, Z. Liu, Q. Li, and D. Wunsch, “Output constrained adaptive controller design for nonlinear saturation systems,” *IEEE/CAA Journal Automatica Sinica*, vol. 8, no. 2, pp. 441-454, 2021.
[30] H. Su, H. Zhang, H. Jiang, and Y. Wen, “Decentralized event-triggered adaptive control of discrete-time non-zero-sum games over wireless sensor-actuator networks with input constraints,” *IEEE Transactions on Neural Networks and Learning Systems*, vol. 31, no. 10, pp. 4254-4266, 2020.
[31] S. Sun, H. Zhang, J. Han, and J. Zhang, “Dissipativity-based finite-time filtering for uncertain semi-Markovian jump random systems with multiple time delays and state constraints,” *IEEE Transactions on Neural Networks and Learning Systems*, vol. 33, no. 7, pp. 2995-3009, 2022.
[32] Y. Wu, H. Ma, M. Chen, and H. Li, “Observer-based fixed-time adaptive fuzzy bipartite containment control for multiagent systems with unknown hysteresis,” *IEEE Transactions on Fuzzy Systems*, vol. 30, no. 5, pp. 1302-1312, 2022.
[33] M. Chen, K. Yan, and Q. Wu, “Multiapproximator-based fault-tolerant tracking control for unmanned autonomous helicopter with input saturation,” *IEEE Transactions on Systems, Man, and Cybernetics: Systems*, vol. 52, no. 9, pp. 5710-5722, 2022.
[34] M. Chen, B. Ren, Q. Wu, and C. Jiang, “Anti-disturbance control of hypersonic flight vehicles with input saturation using disturbance observer,” *SCIENCE CHINA Information Sciences*, vol. 58, no. 7, pp. 070202, 2015.
[35] W. He, X. He, M. Zou, and H. Li, “PDE model-based boundary control design for a flexible robotic manipulator with input backlash,” *IEEE Transactions on Control Systems Technology*, vol. 27, no. 2, pp. 790-797, 2019.
[36] C. Yang, D. Huang, W. He, and L. Cheng, “Neural control of robot manipulators with trajectory tracking constraints and input saturation,” *Automatica*, vol. 32, no. 9, pp. 4231-4242, 2021.
[37] X. Yan, M. Chen, G. Feng, Q. Wu, and S. Shao, “Fuzzy robust constrained control for nonlinear systems with input saturation and external disturbances,” *IEEE Transactions on Fuzzy Systems*, vol. 29, no. 2, pp. 345-356, 2021.
[38] H. Goldstein, *Classical Mechanics*, Cambridge, MA, USA: Addison-Wesley, 1951.
[39] M. C. Rodriguez Linan and W. P. Heath, “Controller structure for plants with combined saturation and deadzone/backlash,” *Proceedings of the 2012 IEEE International Conference on Control Applications (CCA)*, Dubrovnik, Croatia, pp. 1394-1399, 2012.
[40] G. H. Hardy, J. E. Littlewood, and G. Polya, *Inequalities*, Cambridge, U.K.: Cambridge University Press, 1959.
[41] Q. Nguyen and K.-S. Hong, “Simultaneous control of longitudinal and transverse vibrations of an axially moving string with velocity tracking,” *Journal of Sound and Vibration*, vol. 331, no. 13, pp. 3006-3019, 2012.
[42] S. S. Ge and C. Wang, “Adaptive neural control of uncertain MIMO nonlinear systems,” *IEEE Transactions on Neural Networks*, vol. 15, no. 3, pp. 674-692, 2004.
[43] T. Zhou, M. Chen, and J. Zou, “Reinforcement learning based data fusion method for multi-sensors,” *IEEE/CAA Journal Automatica Sinica*, vol. 17, no. 11, pp. 1489-1497, 2020.
[44] Z. Peng, Y. Zhao, J. Hu, R. Luo, B. K. Ghosh, and S. K. Nguang, “Input-output data-based output antisynchronization control of multi-agent systems using reinforcement learning approach,” *IEEE Transactions on Industrial Informatics*, vol. 17, no. 11, pp. 7359-7367, 2021.
[45] C. Deng, C. Wen, W. Wang, X. Li and D. Yue, “Distributed adaptive tracking control for high-order nonlinear multi-agent systems over event-triggered communication,” *IEEE Transactions on Automatic Control*, early access, 2022, doi: 10.1109/TAC.2022.3148384.